JOURNAL OF VIROLOGY, Jan. 1991, p. 232–244
0022-538X/91/010232-13$02.00/0

Vol. 65, No. 1

Transport of Incoming Influenza Virus Nucleocapsids into the Nucleus

KELSEY MARTIN[1] AND ARI HELENIUS[2]*

Department of Molecular Biophysics and Biochemistry[1] and Department of Cell Biology,[2] Yale University School of Medicine, New Haven, Connecticut 06510

Received 13 August 1990/Accepted 9 October 1990

Upon penetration of the influenza virus nucleocapsid into the host cell cytoplasm, the viral RNA and associated proteins are transported to the nucleus, where viral transcription and replication occur. By using quantitative confocal microscopy, we have found that over half of cell-associated nucleoprotein (NP) entered the nucleus with a half time of 10 min after penetration into CHO cells. Microinjection and immunoelectron microscopy experiments indicated that the NP entered the nucleus through the nuclear pore as part of an intact ribonucleoprotein (RNP) structure and that its transport was an active process. Transport of the incoming RNPs into the nucleus was not dependent on an intact microfilament, microtubule, or intermediate filament network. Subsequent to penetration, the matrix (M1) protein appeared to dissociate from the RNP structure and to enter the nucleus independently of the RNP. We found that 50% of penetrated M1 entered the nucleus with a half time of 25 min after penetration into CHO cells. Nuclear transport of M1 appeared to occur by passive diffusion. Entry of incoming M1 into the nucleus was not a prerequisite for infection.

Although the mechanism of penetration of several animal viruses into their host cells is beginning to be understood in some detail (30), virtually nothing is known about how incoming viruses deliver their genomes and associated proteins into the nucleus. Genetic and morphological evidence indicate that adenovirus and herpesvirus nucleocapsids are transported to the nuclear pore and that the viral DNA is then injected into the nucleus, leaving the empty capsid behind in the cytosol (2, 7, 49). Retroviruses, on the other hand, appear to be transported into the nucleus as intact capsid structures containing the reverse-transcribed genome in the form of double-stranded DNA (4). Influenza viruses, which are the topic of this study, deliver their genome into the nucleus for replication in the form of multiple single-stranded RNAs (17, 26). Newly synthesized viral RNA subsequently exits the nucleus of the infected cell to get assembled into virus particles on the plasma membrane. Influenza virus RNA thus displays transport both into and out of the nucleus at different stages of the replication cycle.

The influenza virus nucleocapsid contains eight separate segments of single-stranded, negative-sense RNA. In the virion and in isolated ribonucleoproteins (RNPs), the RNA is in the form of a helix coated with the viral nucleoprotein (NP). Three viral polymerase subunits are also part of the RNP and are located at one end of the elongated rodlike structure (36). Individual RNPs are approximately 15 nm in diameter and between 50 and 130 nm long, depending on the length of the RNA (6, 16, 19). There is evidence that the 3′ and 5′ termini of the individual RNPs interact via complementary sequences and that the RNPs exist consequently as circular structures (18). The viral matrix protein, M1, which forms a shell beneath the viral envelope, has been found to interact with the viral RNPs in biochemical assays (40, 56).

During entry into cells, incoming influenza virus particles first bind to sialic acid-containing receptors on the cell surface. They are then internalized via coated and possibly noncoated endocytic vesicles (32). In the low-pH environment of the endosome, the hemagglutinin (HA) glycoprotein undergoes a conformational change which triggers its membrane fusion activity (48, 52). The viral membrane fuses with the limiting membrane of the endosome and releases the nucleocapsid into the cytosol. This article examines the next steps of viral infection, which deliver the viral RNP to the nucleus.

Our results show that penetration from endosomes occurs about 25 min after internalization. Once released into the cytosol, nucleocapsids undergo decondensation and the RNPs dissociate from the M1 protein. The RNPs thereafter rapidly and efficiently enter the nucleus through the nuclear pores via an active mechanism. They distribute evenly throughout the nucleoplasm except in the nucleolus. Part of the M1 protein also enters the nucleus. Its entry is independent of the RNP and is not essential to infection.

MATERIALS AND METHODS

Cells and viruses. Chinese hamster ovary (CHO) cells were grown as monolayers and passaged biweekly in alpha-minimal essential medium (alpha-MEM) supplemented with 8% fetal calf serum and penicillin-streptomycin (100 U/ml). Madin-Darby bovine kidney (MDBK) and Madin-Darby canine kidney (MDCK) cells were grown as monolayers and passaged biweekly in Dulbecco MEM supplemented with 7% fetal calf serum and penicillin-streptomycin (100 U/ml).

The WSN strain of influenza A virus was obtained from the laboratory of Robert Krug (Rutgers University). Virus stocks were prepared by infecting MDBK cells (90% confluent roller bottles) with 0.01 PFU per cell and collecting the supernatant at 40 h postinfection. The supernatant was divided into aliquots and stored at −70°C for use as virus stock. To purify virus from the supernatant, the virus was first cushioned onto 60% (wt/wt) sucrose in NTE/D_2O (100 mM NaCl–10 mM Tris [pH 7.4]–1 mM EDTA in D_2O) by centrifugation for 90 min at 96,500 × *g* in a Beckman SW28 rotor. The cushioned virus was then purified on a velocity gradient composed of 12.5 to 25% (wt/wt) sucrose in NTE/D_2O and centrifuged for 30 min at 96,500 × *g* in a Beckman

* Corresponding author.

SW28 rotor. It is notable that in our indirect immunofluorescence experiments, nuclear localization of incoming M1 and NP was detected only when purified virus or optimized virus stocks were used. Allantoic fluids from eggs infected with WSN or unpurified stocks from WSN grown at a high multiplicity of infection in MDBK or MDCK cells contained large amounts of free RNPs which were unable to penetrate from the endosomes and gave a predominantly endosomal and lysosomal staining pattern.

To prepare virus labeled with [^{35}S]methionine and [^{35}S]cysteine, we infected 90% confluent MDBK monolayers with 1 PFU per cell for 3 h at 37°C and then labeled them overnight (8 to 12 h) with 200 mCi of [^{35}S]*trans* label (Amersham) per ml. Cells were pelleted at 300 × *g* for 10 min, and the virus was separated from free radioactivity by centrifugation on a discontinuous sucrose gradient of 30 and 60% (wt/vol) sucrose in MNT (20 mM MES [2-4-morpholineethanesulfonic acid]–100 mM NaCl–30 mM Tris) for 3 h at 96,500 × *g* in a Beckman SW28 rotor. After fractionation of the gradient, radioactivity was determined by scintillation counting and the peak fractions were pooled. Over 90% of the labeled NP and M1 remained undegraded after digestion with trypsin, indicating that over 90% of the radioactive virus was intact.

Purified virus was greater than 95% pure, radioactively labeled virus was greater than 90% pure, and stock virus was approximately 60% pure as determined by sodium dodecyl sulfate-polyacrylamide gel electrophoresis (SDS-PAGE) (25). The titer of all virus preparations was determined by plaque assay on MDBK and MDCK cells as previously described (43). On CHO cells, the titer was determined by an infectious center assay. The concentration of purified virus preparations was determined by using the Lowry protein assay (29). The number of virus particles per milliliter was estimated by dividing the protein concentration by the estimated molecular mass of influenza virus (28×10^7 Da) (5). The particle-to-PFU ratio of purified virus was estimated to be 50 to 1 by dividing the number of particles per milliliter by the virus titer (PFU per milliliter).

Antibodies. A polyclonal antibody against whole WSN virus was prepared by immunizing rabbits with detergent and UV-inactivated purified virus. Polyclonal antisera against NP, M1, and HA were prepared by immunizing rabbits with gel-purified protein. Hybridomas which secrete monoclonal antibodies against WSN NP and M1 (46/4 and M2-1C6-4R3) were purchased from the American Type Culture Collection and used to prepare ascites fluids. Monoclonal antibodies against WSN M1 (174/4), WSN HA (431/6), and WSN NP (3/1, 5/1, 150/4, and 469/6) (50, 51) were the gifts of Robert G. Webster (St. Jude's Children's Research Hospital). The four anti-NP ascites were pooled for immunocytochemistry and microinjection. The polyclonal antibody Mprtn, against purified WSN M1 protein, was a gift of Mark Krystal (Mt. Sinai School of Medicine). The monoclonal antibody against nuclear pore proteins, RL1, was a gift of Carol Featherstone and Larry Gerace (Scripps Research Institute) (12, 47). Monoclonal and polyclonal antitubulin antibodies (24), as well as the monoclonal anti-intermediate filament antibody 7A3 (33), were gifts of Thomas Kreis (European Molecular Biology Laboratory). The specificity of all antibodies was confirmed in our laboratory by immunoprecipitation of radioactively labeled virus or cell lysates or both, followed by SDS-PAGE.

Virus internalization conditions. Virus diluted in RPMI 1640 medium, without sodium bicarbonate and supplemented with 0.2% bovine serum albumin–10 mM HEPES (*N*-2-hydroxyethylpiperazine-*N*′-2-ethanesulfonic acid) (pH 6.8), was bound to cells for 90 min at 4°C. The cells were then washed with cold RPMI 1640 medium to remove unbound virus. Medium at 37°C (supplemented with fetal calf serum and containing sodium bicarbonate) was added, and the bound virus was allowed to internalize at 37°C in a CO_2 incubator. Cycloheximide (1 mM) was included in the media during binding and internalization to prevent the synthesis of new viral proteins. This concentration of cycloheximide was shown to block all protein synthesis by radioactive pulse-labeling experiments. In control samples, virus was allowed to bind and internalize in the absence of cycloheximide. In other controls, cells were preincubated with 10 μM monensin for 1 h and then maintained in 10 μM monensin during binding and internalization. Under these conditions, the endosomal pH is raised and viral fusion is blocked (31). To determine the kinetics of penetration, media containing 20 mM NH_4Cl and buffered to pH 7.5 with 20 mM HEPES was added to the cells at various times after internalization. NH_4Cl raises the pH of the endosome within 1 min of addition (38) and thus inhibits viral fusion and penetration.

Kinetics of degradation of incoming viral proteins. WSN virus labeled with [^{35}S]methionine and [^{35}S]cysteine was bound to confluent dishes of CHO cells for 90 min at 4°C and then allowed to internalize for various times at 37°C. The cells were lysed with ice-cold MNT containing 1% Triton X-100, 10 mM chymostatin, 10 mM leupeptin, 10 mM antipain, 10 mM pepstatin, 1 mM phenylmethylsulfonyl fluoride, and 20 mM *N*-ethylmaleimide. The cells were scraped off the dish, 4× sample buffer (800 mM Tris [pH 6.8]–12% SDS–40% glycerol–4 mM EDTA–0.012% bromophenol blue) was added, and the lysates were heated to 95°C for 5 min. The lysates were then analyzed on 10% SDS-polyacrylamide gels, and fluorography was performed on salicylate-impregnated gels with Kodak XAR-5 film. Fluorographs were scanned, and the integrated optical density of bands was determined by using the Visage 2000 densitometer.

Indirect immunofluorescence. Cells were plated on glass coverslips 2 days prior to the experiment. Virus was bound and internalized, and at the indicated time point the cells were washed with ice-cold phosphate-buffered saline (PBS) and fixed for 15 min with 3% formaldehyde in PBS at room temperature. The cells were then quenched for 15 min with 50 mM NH_4Cl in PBS and permeabilized with 0.1% Triton X-100 for 6 min. For surface staining, the cells were fixed and quenched but not permeabilized. Cells were also fixed in absolute methanol for 10 min at −20°C. After fixation, cells were blocked in 10% goat serum made in PBS for 20 min, incubated with the primary antibody at a 1:200 dilution for 30 min, washed, blocked with 10% goat serum-PBS, and then incubated for 30 min in a 1:100 dilution of labeled secondary antibody (fluorescein isothiocyanate [FITC] goat anti-mouse immunoglobulin G [IgG] and/or IgM or Texas red goat anti-rabbit IgG, purchased from Jackson Labs, Tagos, or Zymed). All antiviral primary antibodies were preadsorbed against uninfected cells. Uninfected cells, stained with both primary and secondary or just with secondary antibodies, were included in all experiments as controls. In double-label experiments, cells were incubated with a mixture of both rabbit and mouse primary antibodies during the first antibody incubation and with a mixture of both goat anti-mouse and goat anti-rabbit antibodies during the second antibody incubation. Controls in which cells were incubated with mouse primary antibodies and anti-rabbit secondary anti-

bodies, and vice versa, were done to control for cross-reactivity of the secondary antibodies. The coverslips were mounted in Mowiol (Calbiochemicals) containing 2.5% 1,4-diazobicyclo-[2.2.2]-octane (DABCO) to reduce photobleaching. The coverslips were viewed and photographed on a Zeiss Axiophot microscope. It is worth noting that when cells were fixed with methanol or fixed with formaldehyde and permeabilized with methanol, incoming M1 was no longer found in the nucleus (although newly synthesized M1 was). The staining pattern of incoming NP was the same regardless of the fixation protocol.

Scanning laser confocal microscopy. Specimens were viewed on a Bio-Rad MRC-600 confocal imaging system mounted on a Zeiss Axiovert 10. A 63× objective lens with a 1.4 numerical aperture was used. Confocal settings were: 0.3 mW laser power; zoom 1.5; Kalman filters; 1 s per scan; and 10 frames per image. The photomultiplier gain was set at maximum, and the confocal aperture was adjusted to the smallest size. The single-channel mode was used for single-label experiments, and the dual-channel mode was used for double-label immunofluorescence. The raster size was 512 by 512 pixels. Images of individual cells were collected in three focal planes: through the center of the cell and at the top and bottom surfaces of the cell. The thickness of the optical sections was approximately 0.65 mm. Z-series images, in which optical sections were made at 0.4-mm intervals from the top to the bottom of the cell, were also collected and analyzed at each time point. Equivalent results were obtained as when optical sections at the cell surface and through the middle of the cell were examined.

The amount of fluorescence in the entire cell, the nucleus, and the cytoplasm was quantitated by using the Bio-Rad AREA software. The digital analog of fluorescence intensity on the confocal imaging system is the pixel value. A pixel value of 0 corresponds to minimal intensity, and a pixel value of 255 corresponds to peak intensity. The AREA software thus displays the intensity of fluorescence of a selected area in terms of integrated pixel values. It also displays the size of the area in square millimeters. In each experiment, 10 to 15 cells per time point were analyzed by using the AREA software. Results did not vary significantly between cells or between experiments.

To analyze the colocalization of M1 and NP, images taken of double-labeled cells were normalized to each other, so that the overall fluorescence levels were equivalent, and then the images were subtracted from each other by using the Bio-Rad Subtract function. In subtracted images, the colocalizing M1 and NP are erased, leaving only the signals from the NP and M1 which do not overlap: the white signal represents an excess of NP, and the black signal represents an excess of M1.

Microinjection. Glass capillaries with a 1-mm outer diameter and a 0.58-mm inner diameter (World Precision Instruments) were pulled into microinjection needles on a Sutter micropipette puller (model P-80/PC). Microinjection was done on a Zeiss inverted microscope IM with an Eppendorf microinjector 5242. Microinjection experiments were done in CHO and MDBK cells. The latter were more resistant to the stress of microinjection. Cells were plated onto scored-glass coverslips (Bellco) 48 h before microinjection at a density of 2.5×10^4 cells per ml. Microinjection was performed at room temperature in alpha-MEM containing 20% fetal calf serum, 20 mM HEPES, and penicillin-streptomycin without sodium bicarbonate. Prior to microinjection, antibodies were dialyzed for several hours against 120 mM KCl–10 mM Tris (pH 7.4) (microinjection buffer) and then concentrated in a collodion bag system with a 25-kDa molecular mass cutoff (Schleicher & Schuell) or on a Centricon-30 microconcentrator (Amicon) to approximately 5 to 7 mg of protein per ml. The antibody concentrations were determined by running samples on SDS-PAGE with immunoglobulin standards of known concentration. FITC-conjugated wheat germ agglutinin (WGA) (Sigma) was solubilized in microinjection buffer at a concentration of 10 mg/ml. All samples were centrifuged for 10 min at 13,000 × *g* immediately before microinjection to remove aggregates.

Three different protocols were used in microinjection experiments. In the first, cells were microinjected and allowed to recover for 30 min at 37°C. Virus (20 PFU per cell) was then bound for 90 min at 4°C and internalized for 45 min at 37°C. The cells were fixed, permeabilized, and processed for indirect immunofluorescence. In the second protocol, MDBK cells were infected with WSN virus (20 PFU per cell), and at 1.5 to 2 h postinfection (at which time very little new synthesis of NP or M1 had occurred), the cells were microinjected. Cells were fixed and processed for indirect immunofluorescence 5 h postinfection to look at the location of NP or 7 h postinfection to look at the location of M1. In the third protocol, cells were microinjected, allowed to recover for 30 min at 37°C, and infected with WSN virus (20 PFU per cell). At 5 h postinfection, they were fixed and processed for surface indirect immunofluorescence of HA.

Immunoelectron microscopy. For immunoelectron microscopy, confluent dishes of CHO cells were permeabilized as described (3), except that the nitrocellulose filters were left on the monolayer for only 5 min. Immediately after removing the nitrocellulose filter, the cells were fixed in 3% formaldehyde–PBS for 30 min on ice and then washed in PBS containing 0.01% egg albumin and 50 mM NH_4Cl. The cells were then incubated with mouse or rabbit primary antibodies (1:50 dilution) for 1.5 h at room temperature, washed with PBS, and then incubated overnight at 4°C with 5- or 10-nm gold-conjugated goat anti-mouse or goat anti-rabbit secondary antibodies diluted 1:20 (Janssen). After being washed, the cells were prepared for thin-section electron microscopy essentially as described previously (14). Grids were viewed on a JEOL USA 100 electron microscope.

RESULTS

Penetration of incoming nucleocapsids into the cytoplasm. Before analyzing the transport of viral components from the cytoplasm to the nucleus, it was important to establish how long it takes the viruses to move from the cell surface to the endosomes and to fuse and to determine what fraction of incoming viruses is able to penetrate into the cytoplasm.

To study the kinetics of penetration into CHO cells, we took advantage of an inhibitor, NH_4Cl, which blocks fusion of incoming viruses in endosomes by raising the endosomal pH above the threshold pH needed to activate the HA (55). Viruses were allowed to bind to cells at 4°C at a low multiplicity of infection. A multiplicity of 0.1 PFU per cell was used so that each cell would bind no more than a single infectious virion. At this multiplicity, the Poisson distribution predicted that 90.0% of the cells bound no PFU, 9.5% bound a single PFU, and only 0.5% bound more than 1 PFU. After binding, the cells were warmed to 37°C to allow endocytosis, and 20 mM NH_4Cl was added at various times to block further penetration. To ensure maximal effectiveness of the inhibitor, the medium in which it was added was buffered to pH 7.5 (22). After 5 h, the cells were analyzed by

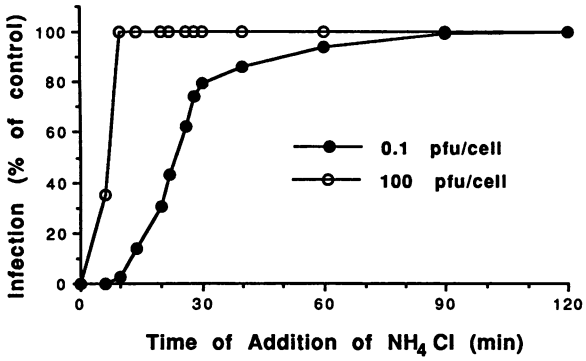

FIG. 1. Kinetics of virus penetration into CHO cells. WSN virus was bound to CHO cells at a multiplicity of infection of 0.1 (●) or 100 (○) PFU per cell. At indicated times postinternalization, medium containing 20 mM NH_4Cl was added. In control cells, no NH_4Cl was added. Five hours after internalization, the cells were fixed and processed for surface indirect immunofluorescence staining of HA. The coverslips were viewed by phase and epifluorescence microscopy, 500 to 600 cells per time point were analyzed, and the percentage of HA positive cells was determined. The results represent the average of three independent experiments.

indirect immunofluorescence for the expression of surface HA, which served as an indicator of infection.

As expected, the extent of infection was highly dependent on the time of NH_4Cl addition. If the inhibitor was added at the time of or a few minutes after warming, virtually no cells expressed HA (Fig. 1, ●). If, on the other hand, the inhibitor was added 90 min postwarming or later, the number of cells infected equaled that observed in inhibitor-free controls. The intermediate time points showed that the majority of the incoming viruses (80%) passed through the step inhibited by NH_4Cl in a time window between 5 to 30 min after warming with a half time ($t_{1/2}$) of 25 min. The remaining 20% continued to penetrate at a slower rate up to 90 min. The apparent lack of synchrony was, most likely, due to differences in the endocytosis rate, intracellular transport, and endosomal acidification between individual cells and endosomes (22).

When performed at a high multiplicity of infection, the same experiment provided an estimate for the minimum time that it takes viruses to penetrate into a cell. This is because only one virus needs to penetrate successfully for infection to occur. Figure 1 (○) shows the time course obtained at a multiplicity of 100 PFU per cell. It is evident that the viruses begin to penetrate within 5 to 10 min after warming.

By using an RNase sensitivity assay, Koff and Knight (23) have estimated that about half of incoming WSN viruses deliver their nucleocapsids into the cytoplasm of MDCK cells. The other half of the viruses presumably fail to fuse and get degraded in the lysosomes. To determine the efficiency of penetration in our CHO cell system, we used an indirect approach by following the intracellular degradation of the structural proteins of incoming viruses that were labeled with [^{35}S]methionine and [^{35}S]cysteine. The incoming HA, which is targeted to the lysosomes regardless of whether the viruses fuse in endosomes or not, was completely degraded within 2 h (Fig. 2). In contrast, only 30 to 35% of M1 and NP were degraded in the same time period. Degradation of these proteins started after an initial lag of about 30 min, followed by relatively rapid degradation up to 2 h, followed by a slower phase. At 6 h after internalization, 31% of incoming M1 and 57% of incoming NP remained

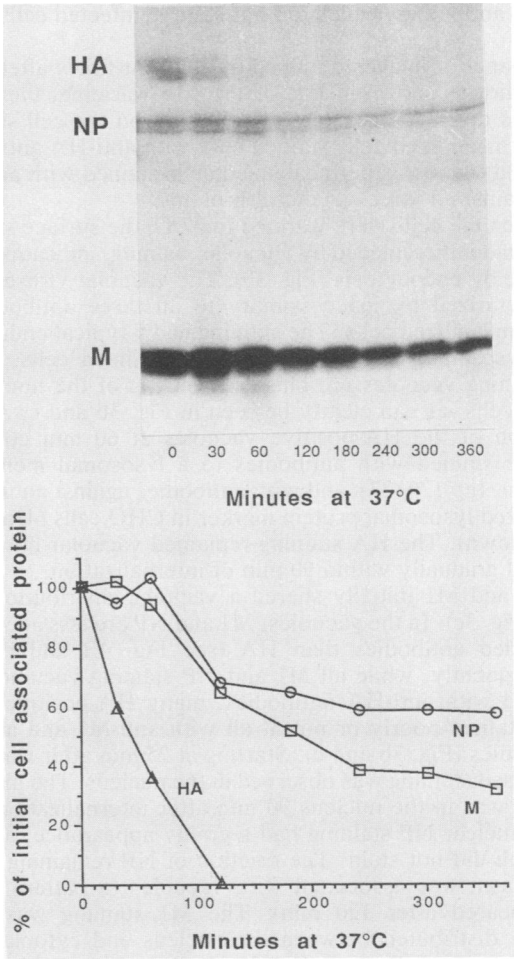

FIG. 2. Kinetics of degradation of structural proteins in CHO cells. Virus labeled with [^{35}S]methionine and [^{35}S]cysteine was added to confluent 60-mm dishes of CHO cells (10^5 cpm per dish). At the indicated times postinternalization, the cells were lysed and whole cell lysates were analyzed by SDS-PAGE on 10% nonreduced gels. After fluorography, the amount of HA, M1 (labeled M), and NP at each time point was quantitated by densitometry and normalized to the amount present at 0 min. Note that NP runs as a doublet. The minor bands just below NP and M1 in the 0-, 30-, and 60-min time points represent HA1 and HA2. This experiment was repeated three times, with equivalent results.

intact in the cell. We expect that this slowly degraded fraction represents the M1 and NP which penetrated from endosomes into the cell.

These results suggest that 65 to 70% of bound virus penetrated into the cytoplasm in CHO cells. The $t_{1/2}$ of penetration was 25 min after warming, and the rate of degradation, particularly of NP but also of M1, was slow.

Distribution of incoming viral proteins. Indirect immunofluorescence with antibodies to NP, M1, and HA was employed to determine the distribution of the incoming viral proteins. Influenza virus at a multiplicity of infection of 40 PFU per cell was bound to cells in the cold and allowed to enter for various times at 37°C. Cycloheximide (1 mM) was present to block the synthesis of new proteins. The cells were fixed and processed for indirect immunofluorescence with or without prior permeabilization. Mono- and poly-

clonal antibodies, which did not stain uninfected cells, were used.

A panel of images obtained at different times after internalization is shown in Fig. 3. Prior to warming, the bound viruses displayed a patchy distribution on the cell surface. Unpermeabilized cells stained only with anti-HA antibodies (Fig. 3a), whereas permeabilized cells stained with antibodies against all three structural proteins.

When the cells were warmed to 37°C, the surface staining was gradually replaced by vacuolar staining, indicating virus uptake by endocytosis (Fig. 3b). The vacuolar viruses were characterized by inaccessibility to all three antibodies in unpermeabilized cells. The staining had a typical endosomal and lysosomal morphology in permeabilized cells. Virus-containing vacuoles are clustered on top of the nucleus in CHO cells, as can clearly be seen in Fig. 3b and c. A large fraction of the HA-positive vacuoles at 60 min could be double stained with antibodies to a lysosomal membrane protein, Igp 120 (27), and with antibodies against an uncharacterized lysosomal protein marker in CHO cells (43a) (data not shown). The HA staining remained vacuolar but disappeared gradually within 90 min of internalization.

NP and M1 initially shared a vacuolar distribution with HA (Fig. 3c). In the vacuoles, M1 and NP are less accessible to added antibodies than HA (see Fig. 4B and below). Consequently, while all M1 and NP staining vacuoles also stained with anti-HA antibodies, many HA-positive vacuoles stained poorly or not at all with anti-M1 and anti-NP antibodies (Fig. 3b and c). Starting at 25 min after warming, increased staining was observed in the nucleus. The majority of NP was in the nucleus 90 min after internalization (Fig. 3d). Nuclear NP staining had a grainy appearance, and the nucleoli did not stain. The fraction of NP remaining in the cytoplasm was associated with vacuoles (a pattern which disappeared after 120 min). The M1 staining was more evenly distributed between the nucleus and cytoplasm 90 min after internalization (Fig. 3e). In the nucleus, M1 stained homogeneously throughout the nucleoplasm. Cytoplasmic M1 protein gave a diffuse staining as well as a filamentous cytoskeletal staining. The latter represented M1 protein bound to microfilaments because it overlapped with actin when double-stained with Texas red-labeled phalloidin (data not shown). It is important to note that incoming (but not newly synthesized) M1 protein remained entirely cytoplasmic in MDBK and MDCK cells (data not shown). The extent of incoming M1 entry into the nucleus is therefore cell type dependent.

The efficiency and kinetics of nuclear uptake of NP and M1 were analyzed quantitatively by confocal microscopy. Images were recorded of optical sections at the surface and through the middle of the cell, and the amount of fluorescence in the nucleus was quantitated by use of the Bio-Rad AREA software. Nuclear NP staining reached its half-maximal level at 33 to 35 min and its maximal staining at 60 min after internalization (Fig. 4A). Two hours after internalization, 80% of cell-associated NP staining was in the nucleus. The entry of M1 protein into the nucleus was less efficient than that of NP: quantitation with the confocal microscope showed a maximum of 50% of the M1 staining in the nucleus. Uptake was also somewhat slower, with a $t_{1/2}$ of about 50 min and a maximum at 120 min (Fig. 4A). In cells treated with monensin, a carboxylic ionophore which like NH_4Cl prevents viral penetration (31), the staining of NP and M1 remained entirely vacuolar (Fig. 3f) and infection did not occur.

The overall staining patterns observed were the same over a wide range of multiplicities of infection (3 to 500 PFU per cell). The limit of detection by indirect immunofluorescence corresponded to 3 PFU per cell which, given the estimated particle-to-PFU ratio of our virus, represents 150 virus particles per cell. Attempts to visualize the incoming polymerase molecules (PB1 and PB2) by using specific antibodies failed even at the highest multiplicities. This was most likely due to the low abundance of antigen.

Taken together, the immunofluorescence experiments indicated that a large fraction of the incoming NP and M1 entered the nucleus shortly after penetration into the cytoplasm. When compared with the kinetics of penetration (Fig. 1), it was evident that it took no longer than 10 min for NP and 25 min for M1 to move from the endosomes to the nucleus. While virtually all of the penetrated NP entered the nucleus, M1 partitioned between the nucleus and cytosol.

M1 and NP separate after penetration. The confocal images were also analyzed by using the Bio-Rad Subtract function to determine to what extent NP and M1 were colocalized at different stages of entry. At early times, when the viruses were still on the surface and in the endosomes, the two proteins were clearly colocalized (Fig. 5a). Beginning at 20 min after internalization and increasing thereafter, they separated from each other, judging by the appearance of extensive white areas (excess NP over M1) and black areas (excess M1 over NP) in the subtracted images (Fig. 5b and c). Apparently, the M1 protein dissociated from the RNPs shortly after penetration into the cytosol. The abundance of black vacuolar images at 30 min (Fig. 5b, arrows) suggested that some of the M1 remained associated with the vacuoles longer than NP. This may explain the slower entry of M1 into the nucleus.

A quantitative analysis of confocal images revealed a dramatic increase in overall NP and M1 fluorescence after penetration (Fig. 4B). The specific immunofluorescence increases were fourfold for NP and ninefold for M1. The specific HA fluorescence, in contrast, showed no increase. The time course suggested that the effect coincided with penetration and nuclear uptake (Fig. 4B). The most likely explanation was that M1 and NP are so compactly packaged in the intact virus particles that antibodies have limited access to the antigens even though the membrane is permeabilized by detergent. When released into the cytoplasm, the structures might be decondensed and the antigenic epitopes would become more accessible. Dissociation of M1 from the RNPs and separation of individual RNPs from each other may also contribute to the increased accessibility of both antigens.

Blocking nuclear entry with antibodies. In a series of microinjection experiments, we next determined whether the transport of incoming viral proteins could be inhibited by cytosolic antibodies and whether such antibodies blocked productive infection. The injected antibodies were mouse monoclonals against M1 and NP, respectively. Cells were injected with the antibodies and then infected with influenza virus. Two different protocols were employed thereafter. To determine whether the antibodies blocked nuclear import of the viral proteins, the cells were fixed 45 min after internalization and double stained with FITC goat anti-mouse antibody (to detect the injected cells) and rabbit anti-M1 or anti-NP antibody followed by Texas red goat anti-rabbit antibody (to visualize the incoming viral proteins). To determine whether the injected antibodies were inhibitory to infection, the injected and infected cells were incubated for 5 h and then subjected to surface indirect immunofluorescence by using anti-HA antibodies to detect newly synthe-

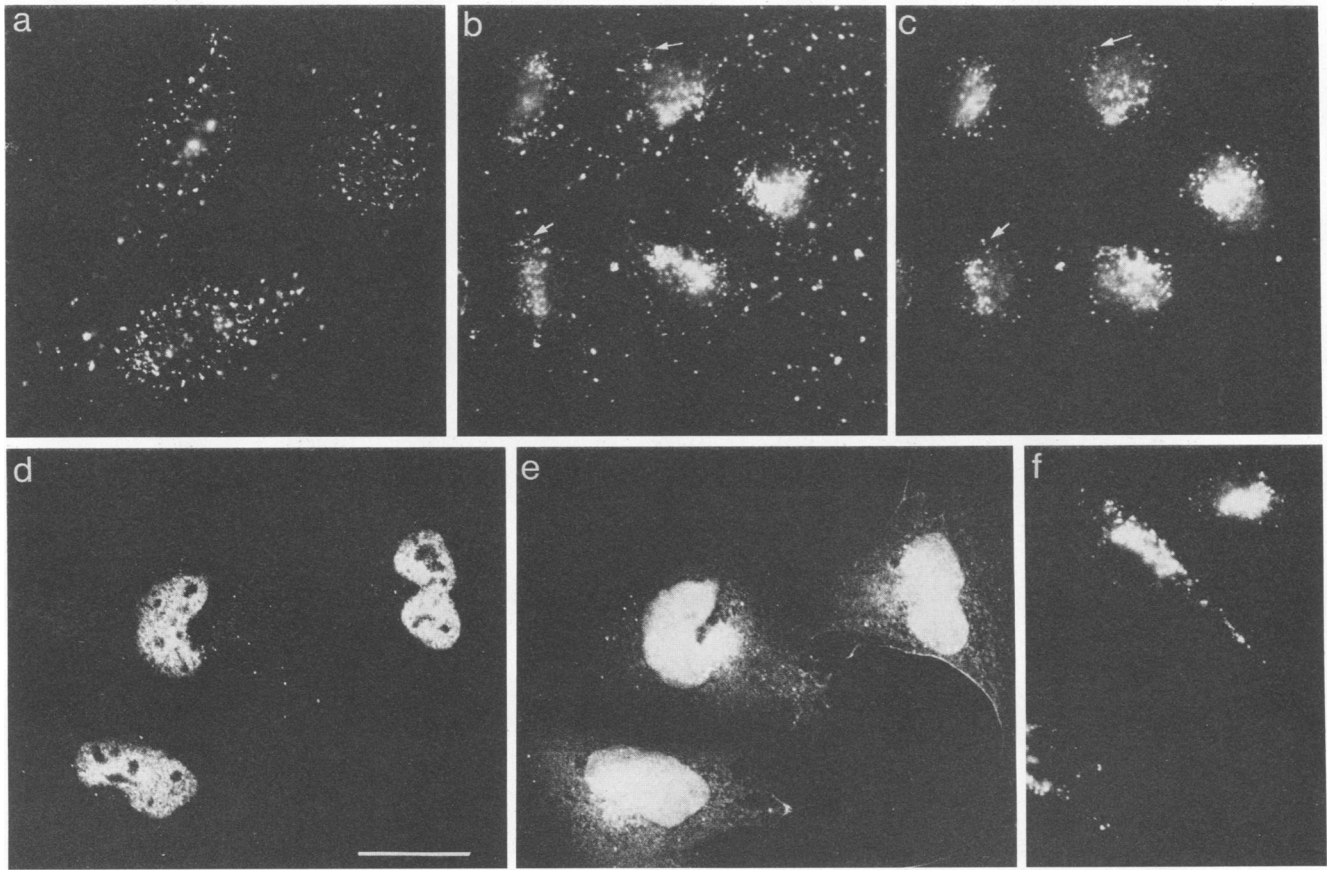

FIG. 3. Localization of incoming HA, M1, and NP in CHO cells. Purified WSN virus was added to CHO cells at a multiplicity of infection of 40 PFU per cell in the presence of 1 mM cycloheximide. The cells were fixed (a) or fixed and permeabilized (b through f) and then stained with monoclonal anti-HA (a and b), a pool of four monoclonal anti-NP antibodies (d and f), or polyclonal anti-M1 antibodies (c and e). At 0 min (after binding for 90 min at 4°C but before internalization), HA was on the surface of unpermeabilized cells (a). At 20 min after internalization, HA (b) and M1 (c) were in intracellular vacuoles. At 90 min after internalization, NP (d) was in the nucleus, while M1 (e) was distributed between the nucleus and cytoplasm. In control cells, in which virus was internalized for 60 min in the presence of 10 mM monensin, NP staining was restricted to intracellular vacuoles (f). Note that panels b and c and panels d and e show the same cells double labeled with anti-HA and anti-M1 (arrows point to examples of double-labeled vacuoles) or with anti-NP and anti-M1, respectively. Bar, 25 mm.

sized HA. Controls showed that the presence of anti-NP or anti-M1 did not affect expression of HA if the antibody was injected 2 h after infection. Any effect of the injected antibodies can therefore be ascribed to early events in infection.

Examples of the microinjection studies are shown in Fig. 6, and all of the results are summarized in Table 1. Antibodies against NP in the cytosol were found to block transport of incoming (and also, incidentally, when microinjected 1.5 to 2 h postinfection, newly synthesized) NP into the nucleus (Fig. 6a and b). They also blocked infection as measured by HA expression (Fig. 6g). Antibodies against NP did not block the entry of M1 into the nucleus. Antibodies against M1, while inhibitory to the entry of M1 into the nucleus, had no effect on NP import into the nucleus (Fig. 6c and d) or on infection. Microinjected control antibodies (rabbit polyclonal antisera and mouse monoclonal ascites fluid) did not block nuclear import of NP or M1 nor did they inhibit infection.

These results confirmed that M1 and NP are independently transported to the nucleus. They also showed that transport of M1 into the nucleus is not required for replication and transcription of viral RNA, while transport of NP into the nucleus is required. Indirectly, this implies that NP enters the nucleus as part of the viral RNPs.

Route of entry into the nucleus. The rapid transport of NP into the nucleus suggested that transport from the endosomes to the nucleus could be mediated by microfilaments or microtubules. We found that disruption of these filaments with cytochalasin D (20 mM) and Nocodazol (10 mM) had no effect on NP or M1 uptake into the nucleus nor on infection (data not shown). That the filaments were indeed disrupted by the agents was confirmed by immunofluorescence. It has been suggested that nuclear pores may be associated with intermediate filaments (15). We therefore injected specific monoclonal anti-intermediate filament antibodies which collapse the intracellular intermediate filament network (33). Under these conditions, we did not observe inhibition of either M1 or NP entry into the nucleus (Fig. 7c). Note in Fig. 7b that the intermediate filaments have collapsed into the center of the microinjected cells. In summary, we found that microtubules, intermediate filaments, and microfilaments were not essential for nuclear uptake of influenza virus components.

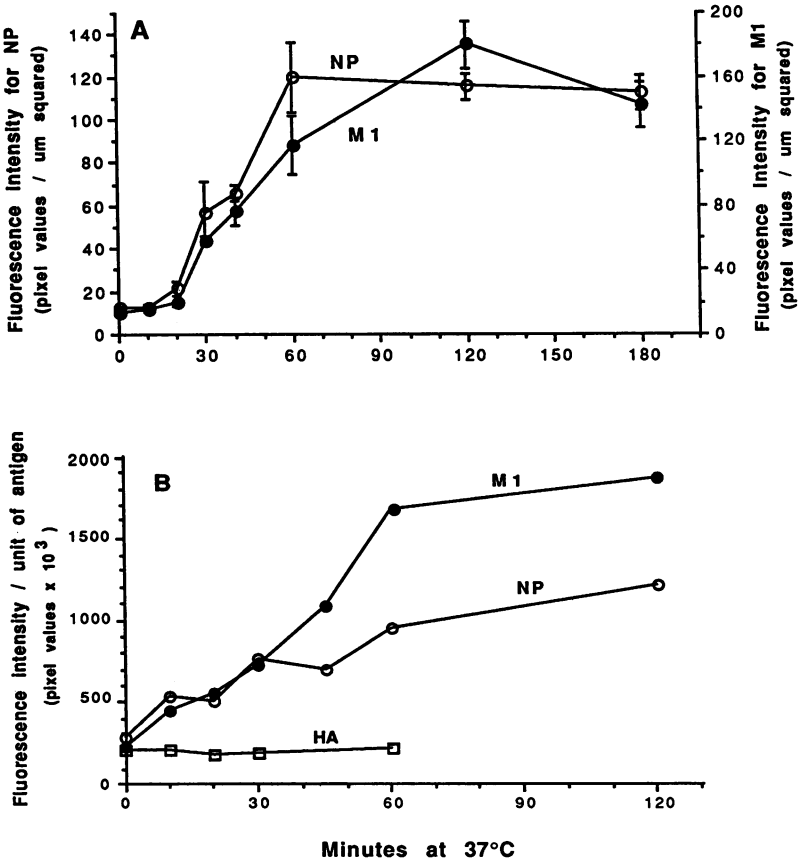

FIG. 4. Quantitation of nuclear and cellular M1 and NP staining. Cells treated with WSN virus were fixed, permeabilized, and stained as in Fig. 3. The slides were viewed on a Bio-Rad confocal microscope (model MRC-600). (A) The amount of fluorescence in the nuclei was determined by using the AREA software. The datum points represent the average of four independent experiments. The error bars represent standard deviations. Similar results were obtained when cells were infected with 10 or 100 PFU per cell or when nuclear NP was quantitated in methanol-fixed cells. (B) Total cellular immunofluorescence as a function of time. By using the AREA software, the total cellular HA, M1, and NP immunofluorescence at indicated time points was determined. To obtain the immunofluorescence per unit antigen, the observed level of immunofluorescence was multiplied by the fraction of undegraded antigen remaining in the cell at each time point (see Fig. 2).

We performed a series of microinjection experiments to determine whether the viral RNP entered the nucleus through nuclear pores. A monoclonal antibody (designated RL-1) prepared against nuclear pore components by Snow et al. (47) and WGA were injected into the cytosol. Both RL-1 and WGA have been shown to inhibit active transport of molecules through the nuclear pore without affecting passive diffusion (12, 13, 54). The RL-1 antibodies stained the nuclear membrane of CHO cells (Fig. 6e). Examples of microinjected cells are shown in Fig. 6e and f, and the effects of these reagents of virus entry are included in Table 1. We found that transport of incoming (and newly synthesized) NP into the nucleus was fully inhibited by WGA and considerably reduced by RL-1. RL-1 also blocked infection as measured by HA expression on the cell surface. Neither RL-1 nor WGA blocked entry of M1 into the nucleus.

These results showed that transport of NP and M1 from the endosome to the nucleus was independent of the major cytoskeletal elements. NP entered the nucleus via the nuclear pores. In contrast, the entry of the M1 protein was either independent of nuclear pores or mediated by passive diffusion. Given the small size of the M1 protein in its monomeric form, the latter explanation seemed more likely.

Visualizing the passage of NP and M1 from endosome to nucleus. Immunocytochemistry at the electron microscopic level was used to track the incoming NP and M1 in the cytoplasm. The technique used involved permeabilization of the plasma membranes to gain access to antigens localized on the cytosolic surface of cellular organelles (14). CHO cells grown on a monolayer were infected with WSN virus and overlaid with a nitrocellulose filter as previously described (3, 45). When the filter was peeled away, patches of the plasma membrane were ripped off. Soluble cytoplasmic molecules thereby leaked out while larger structures and organelles remained in place, accessible to externally added antibodies. After being labeled with secondary antibodies coupled to colloidal gold, the cells were fixed with glutaraldehyde and processed for thin-section electron microscopy by standard procedures.

Cells that had internalized viruses for 30 min showed NP staining in electron-dense clusters on the cytoplasmic face of endosomes (Fig. 8a). The endosomes frequently contained unfused influenza virus particles. Each cluster usually contained 6 to 10 gold particles, and the dimensions of the stained structures were approximately 30 to 80 nm, which is consistent with the reported size of individual influenza virus RNPs (6, 16, 19). Clusters with NP staining were also observed at the cytoplasmic entrance to nuclear pores (Fig.

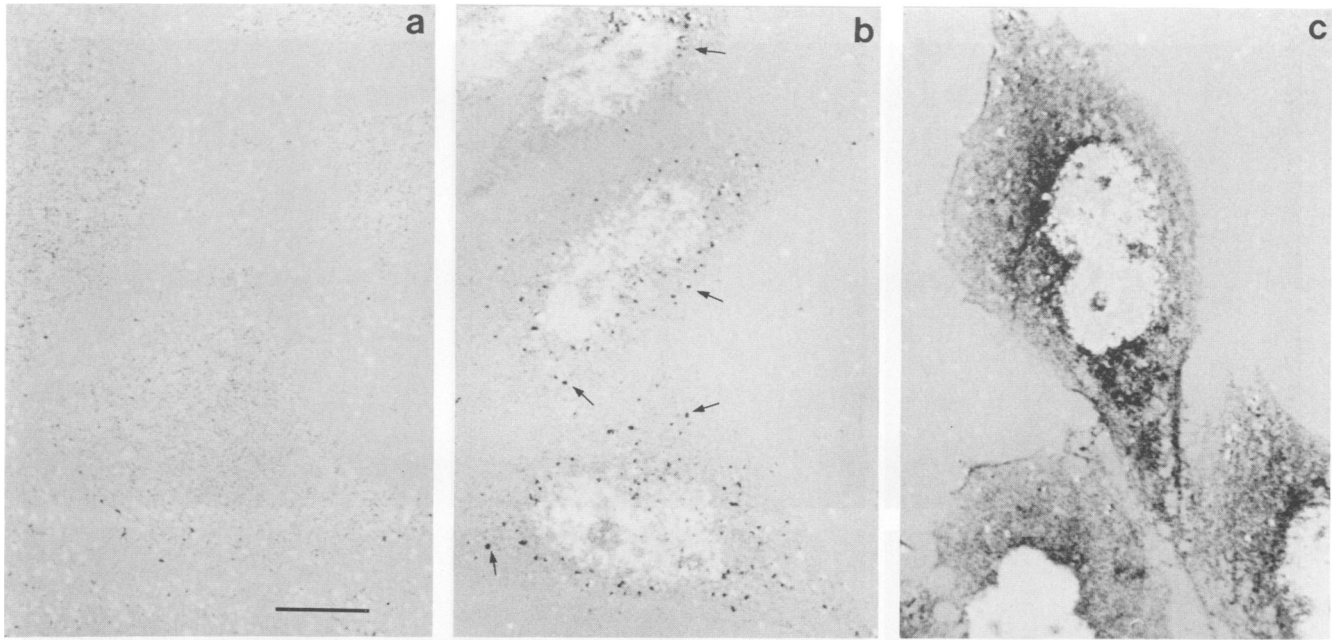

FIG. 5. Subtracted images from the confocal: M1 and NP separate after penetration. Specimens prepared as described in the legend to Fig. 3 were viewed on a Bio-Rad confocal microscope (model MRC-600). The M1 and NP images were collected and subtracted from one another by using the Bio-Rad Subtract function. Where M1 and NP colocalized, the signal was gray; where there was an excess of M1, the signal was black; and where there was an excess of NP, the signal was white. The times after internalization were 0 (a), 30 (b), and 120 (c) min. Arrows in panel b point to vacuolar M1 staining. Bar, 10 mm.

8b), confirming that they serve as sites of NP entry. The endosomal and nuclear pore staining were detectable as late as 90 min after virus entry in the presence of cycloheximide, consistent with the nonsynchronous time course of virus penetration (Fig. 1). No staining was observed in monensin-treated control cells, demonstrating that the cytosolic staining pattern observed was dependent on penetration. Gold particles could be seen only occasionally in the nucleoplasm (see Fig. 8c) by using this technique. The reason for the lack of labeling in the nucleus was probably inefficient penetration of antibodies through the nuclear membranes. The nucleus was found to contain large amounts of NP (and M1) by indirect immunofluorescence and by frozen thin-section immunocytochemistry (data not shown).

When the permeabilized cells were stained with antibodies against M1, labeling could be seen on the cytoplasmic surface of endosomes (Fig. 8d), on the nuclear envelope (Fig. 8e), and sometimes in the nucleus (Fig. 8d). Labeling of nuclear pore was rarely seen. Overall, there was less M1 staining than NP staining, suggesting that a larger fraction of M1 leaked out during the permeabilization. Monensin-treated and permeabilized control cells did not stain with anti-M1 antibodies.

These observations provide morphological evidence that NP moves from the cytoplasm to the nucleus via the nuclear pore. The size of the labeled structures supports the interpretation that NP was transported into the nucleus as part of the RNP complex.

DISCUSSION

In this report we have extended our studies of influenza virus entry to include events subsequent to the fusion of the viral and endosomal membranes. Our results allow us to outline several steps. The virus penetrates from endosomes into the cytoplasm by acid-induced fusion. Next, the viral RNPs separate from the M1 protein and enter the nucleus through the nuclear pores. The transport is an active process presumably mediated by signals in the NP protein. The incoming M1 protein distributes between the nucleus and the cytoplasm. It enters the nucleus more slowly and less efficiently than NP, and its entry is not a prerequisite for infection.

The penetration into the cytosol and the subsequent transfer of NP into the nucleus are rapid and efficient processes. Our results indicated that, once the cells have been warmed to 37°C, penetration of viruses from acidic endosomes starts after 6 min and continues for about 80 min with a $t_{1/2}$ of 25 min. This time course, as well as the pH dependence of WSN virus fusion (55), suggests that penetration occurs predominantly from late endosomes (34). In CHO cells, the late endosomes are located in the perinuclear region of the cytoplasm. We estimated that 65 to 70% of the incoming virus penetrated into the cytoplasm, with the rest being degraded in lysosomes. While the incoming HA is relatively rapidly degraded, most of the NP and M1 are stable in the cell for several hours. The process of penetration in CHO cells was somewhat faster and more efficient than that previously reported in MDCK cells by Koff and Knight (23) and in primary macrophages by Meyer and Horisberger (35). The difference may be explained by cell type variability. In support of this possibility, we found that virus endocytosis and nuclear transport of NP were slower and less complete in MDCK and MDBK cells than in CHO cells (unpublished observations).

Virtually all of the NP released into the cytosol of CHO cells entered the nucleus. Uptake occurred with a $t_{1/2}$ of 33 to 35 min after warming, which means that the time between penetration into the cytosol and entry into the nucleus was

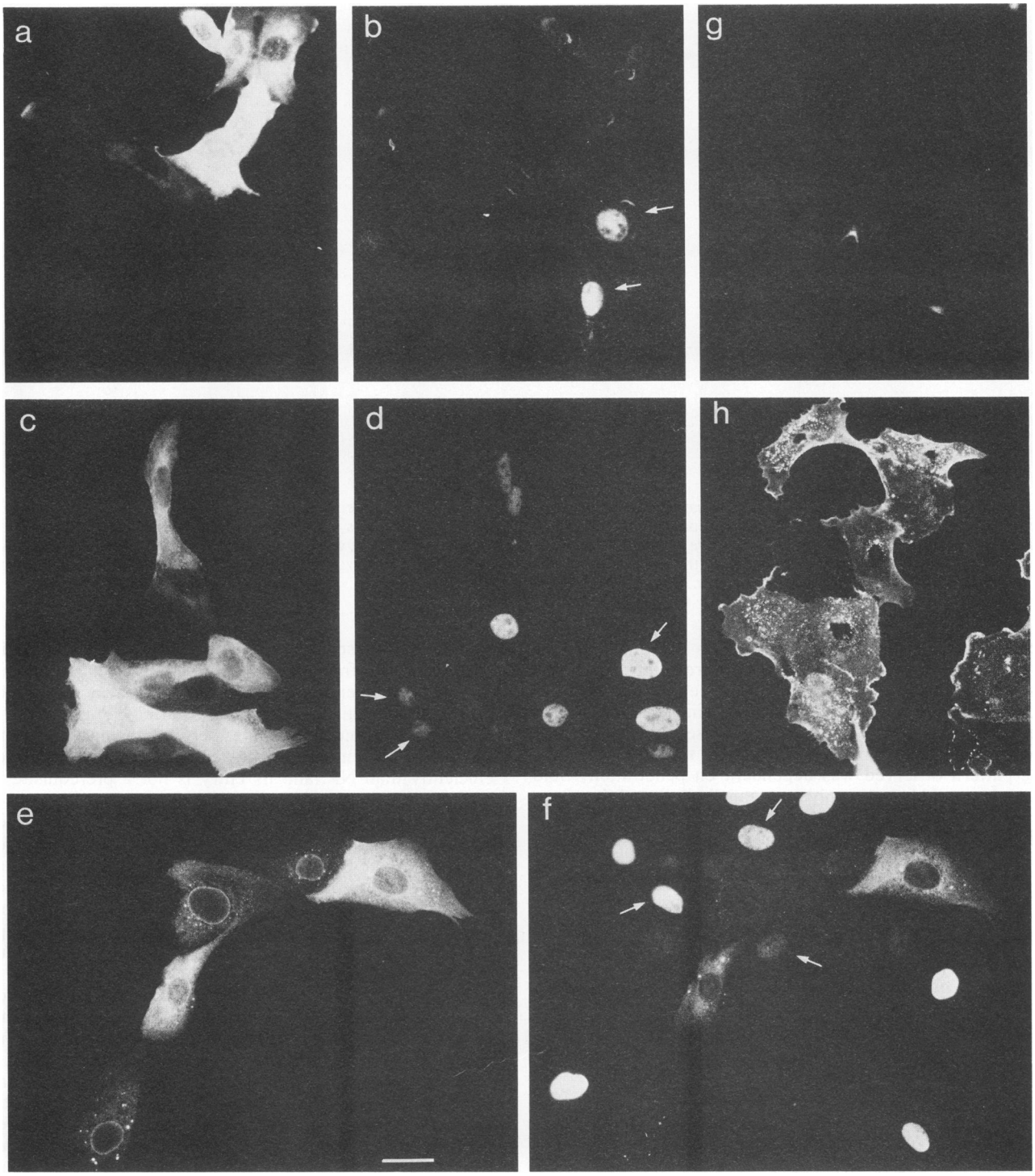

FIG. 6. Effect of microinjected antibodies on influenza virus infection. To determine the effect of microinjected antibodies on nuclear transport, mouse monoclonal antibodies against NP (a), M1 (c), or nuclear pore components (e) were injected into CHO (a and b) or MDBK cells (c, d, e, and f). WSN virus (20 PFU per cell) was subsequently bound to the cells and allowed to internalize for 45 min. The cells were fixed, permeabilized, and stained with rabbit polyclonal anti-NP antibody (b, d, and f) followed by FITC goat anti-mouse IgG (to detect the injected antibody) and Texas red goat anti-rabbit IgG. Note that the uninjected cells (b, d, and f, small arrows) served as internal controls. To determine the effect of microinjected antibodies on infection, MDBK cells were microinjected with a pool of mouse monoclonal antibodies against NP (g) or with a rabbit polyclonal anti-M1 antibody (h). They were then incubated with 20 PFU of WSN virus per cell. After 5 h, the cells were fixed and stained with a mouse monoclonal anti-HA antibody followed by FITC goat anti-mouse IgG. Because the cells were not permeabilized in panels g and h, we did not visualize the microinjected antibodies. Bar, 20 mm.

TABLE 1. Effect of microinjected antibodies and lectins on nuclear import and infection[a]

Microinjected molecule	Antigen recognized[b]	Nuclear import				Infection[c]
		Incoming NP	Incoming M1	Newly synthesized NP	Newly synthesized M1	
Anti-NP	NP	−	+	−	+	−
Anti-M1	M1	+	−	+	−	+
RL-1	Nuclear pore	−	+	ND[d]	ND	−
WGA	Nuclear pore	−	+	ND	ND	−
7A3	Intermediate filament	+	+	ND	ND	ND
CG1[e]	Chromaffin granules	+	+	+	ND	+
Rabbit preimmune sera		+	+	+	ND	+

[a] Cells were microinjected with the indicated molecule. The effect on nuclear import of incoming or newly synthesized NP and M1 and on infection was assayed as described in Materials and Methods.
[b] Antigen recognized by the microinjected antibody or lectin.
[c] Infection was assayed by the presence of HA on the surface of cells 5 h postinternalization.
[d] ND, Not done.
[e] CG1, Mouse monoclonal ascites fluid.

no more than 10 min. The M1 protein also entered the CHO cell nucleus but more slowly and less efficiently. The final distribution of M1 was therefore half in the cytosol and half in the nucleus. Interestingly, we found that the fate of incoming M1 was also cell type dependent: the incoming M1 failed to enter the nucleus in MDBK and MDCK (unpublished results). Newly synthesized M1, however, was capable of entering the nucleus quite efficiently in all three cell lines. Thus, the properties of incoming and newly synthesized M1 may be different.

The efficiency of NP penetration into the cytoplasm and transport into the nucleus was somewhat surprising in view of the high particle-to-PFU ratio of influenza virus. We estimated that approximately one of four viruses initially added to the culture reached the nucleus. The particle-to-PFU ratio indicated, on the other hand, that only 1 of 50 particles was infectious. In other words, on average, 10 viruses had to enter the nucleus in order to productively infect the cell. Our results suggest that the inefficiency cannot be due to inefficient entry. The inefficiency could be explained by incomplete packaging of the eight RNP strands into viral particles, so that only some of the particles would contain the complete genome.

The intracellular distribution and differential kinetics of transport of M1 and NP into the nucleus indicated that they dissociated from each other soon after penetration. This was confirmed by immunocytochemistry. Thus, while newly synthesized M1 protein has a strong affinity for viral RNPs (31a), the incoming M1 is no longer tightly bound. The change in affinity between the structural proteins may be crucial not only for the dissociation of the incoming viral core particle, but also for allowing the entry of RNPs into the nucleus. We have found that newly synthesized RNPs in the nucleus of infected cells associate with M1 protein before transport into the cytosol. In contrast, the incoming RNPs do not contain detectable M1 when they enter the nucleus. This raises the possibility that the association between M1

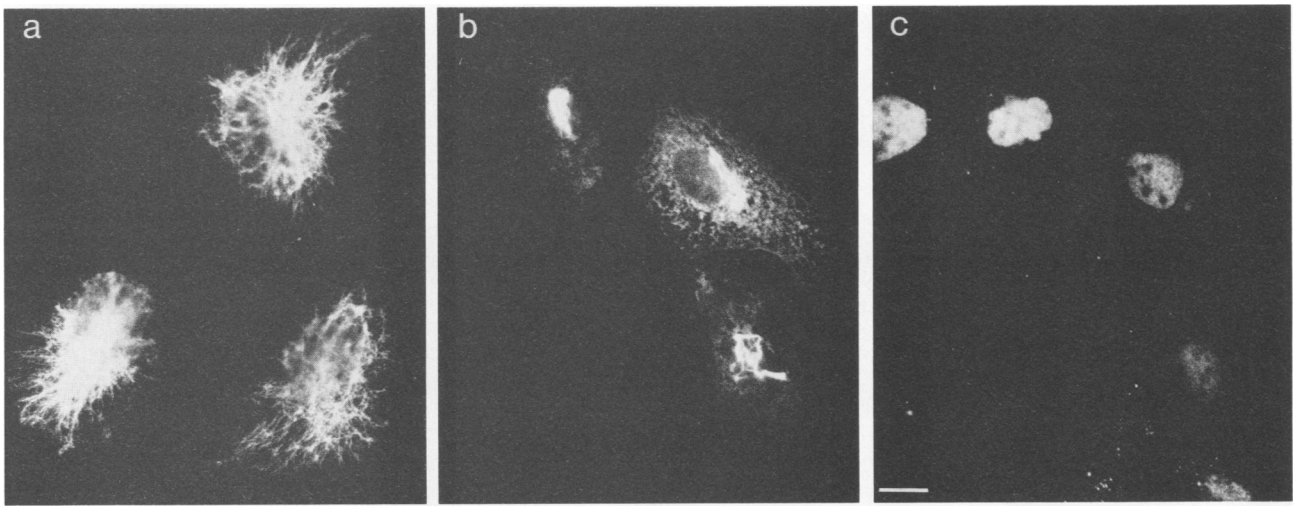

FIG. 7. The intermediate filament network is not required for transport of NP to the nucleus. CHO cells were microinjected with 7A3, a monoclonal antibody against intermediate filaments. The cells were allowed to recover for 1 h at 37°C (at which time the intermediate filament network was collapsed). WSN virus (20 PFU per cell) was bound and allowed to internalize for 30 min. The cells were fixed, permeabilized, and stained with polyclonal rabbit antibodies against NP (c), followed by Texas red goat anti-rabbit IgG and FITC goat anti-mouse IgG to detect the anti-intermediate filament antibodies in microinjected cells (b). The intermediate filament network has collapsed to the center of the cell in microinjected cells (b). As a control, uninjected CHO cells were fixed, permeabilized, and stained by indirect immunofluorescence with anti-intermediate filament antibodies to show the intact intermediate filament network (a). Bar, 20 mm.

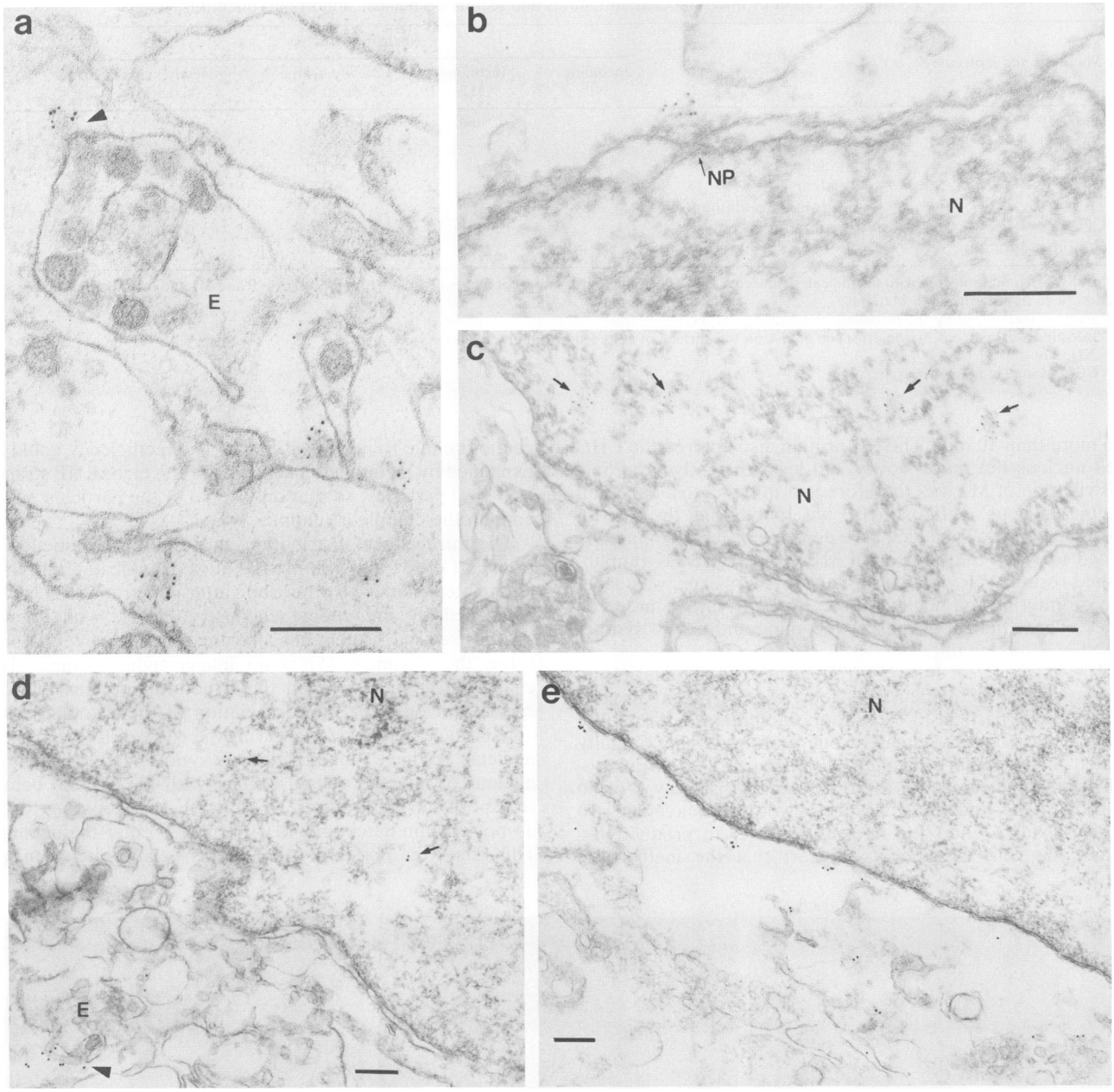

FIG. 8. Immunoelectron microscopy of nitrocellulose-permeabilized cells. WSN virus (5,000 PFU per cell) was bound to confluent 60-mm dishes of CHO cells and allowed to internalize for 30 min. The cells were disrupted with nitrocellulose filters, fixed, and incubated with a pool of monoclonal anti-NP antibodies followed by 5-nm gold-conjugated goat anti-mouse (a, b, and c) or with polyclonal anti-M1 antibodies followed by 10-nm conjugated goat anti-rabbit (d, e, and f). The cells were then processed for thin-section electron microscopy. NP and M1 staining structures are seen at the site of endosome (E)–virus fusion (a and d, arrowheads), and in the nucleus (N) (c and d, arrows). NP staining structures are seen at the cytoplasmic face of nuclear pores (NP) (b), while M1 is seen in association with the nuclear envelope (e). Bars, 0.2 mm.

protein and RNPs modulates the directionality of RNP transport between the nucleus and the cytosol.

One of the consequences of the penetration reaction and of the subsequent dissociation of the core components was a dramatic increase in the immunofluorescence signal for both NP and M1 (Fig. 4B). The $t_{1/2}$ of this change, approximately 28 min for NP and 40 min for M1, indicated that it took place after penetration but before nuclear uptake. Quantitative analysis of fluorescence signals from incoming structural proteins may, in the future, provide a general approach for investigating the penetration and uncoating of viruses. Uncoating and disassembly may result in increased or modified antigenic properties of many viruses.

While we have thus far been unable to directly follow the entry of the incoming viral RNA, we are confident that they enter the nucleus as RNPs, i.e., complexed with NP and the viral RNA-polymerase proteins. Whenever NP entry into the nucleus was blocked by cytosolic antibodies, infection

was also inhibited. The size of the cytoplasmic complexes stained with anti-NP (30 to 80 nm) was consistent with particles in the size range of single, individual RNPs (6, 16, 19). Furthermore, the diameter of single RNP particles is clearly compatible with the functional diameter of the nuclear pores (27 nm) (10, 11), while the intact complete nucleocapsid with all RNPs would be too large to enter. The fact that the influenza virus genome is segmented may, in fact, allow its entry into the nucleus. We have made numerous biochemical attempts to demonstrate and quantitate viral RNA and structural protein entry into the nucleus. These attempts have failed because of the fragility of isolated nuclei and nonspecific background binding of RNPs to the broken nuclei.

NP was found to enter the nucleus through the nuclear pores. It was inhibited by the RL-1 antibody and by WGA, which selectively block active transport of proteins through the pores (12, 13). As far as size is concerned, monomeric M1 protein and even monomeric NP could enter the nucleus passively with the kinetics observed (39). The entry of M1 into the nucleus was, indeed, insensitive to the RL-1 antibody and WGA, suggesting that it occurred by passive diffusion.

Active transport into the nucleus is signal mediated and ATP dependent (9, 21, 37, 41). All four RNP-associated proteins, i.e., NP, PA, PB1, and PB2, are known to enter the nucleus when expressed individually in cells, demonstrating that each contains the signals required for nuclear transport and retention (20, 28, 46). While any one of these proteins could be responsible for the targeting of the incoming RNPs to the nucleus, the most important protein is probably NP because it is the only protein present on the RNPs in high copy number (one NP per 20 nucleotides) (6). Multiple transport signals are known to increase the rate of protein uptake into the nucleus (11, 42). The high number and density of NP molecules in the RNP particle could explain the rapid uptake kinetics observed. A nuclear localization sequence has already been identified in NP (8). Since mutant NP molecules lacking the functional signal enter the nucleus as quickly as the wild type but fail to accumulate (8), the signal may, however, serve as a retention signal rather than a targeting signal. Another as-yet-unidentified sequence may thus be responsible for targeting into the nucleus.

The transport of NP into the nucleus was not dependent on elements of the cytoskeleton. No significant change was observed after disrupting the microfilaments, the microtubules, or the intermediate filament network. This may suggest that the transport from the endosome to the nuclear pore is passive. To what extent it depends on cellular receptor proteins (1, 44, 53) and other functions remains to be seen.

The studies reported here have extended our understanding of the entry pathway of influenza virus, and they have established methods for studying nuclear transport in viral systems. A unique feature of influenza virus RNP nuclear transport is its bidirectionality: incoming RNPs are transported into the nucleus at the start of infection and newly synthesized RNPs are transported out of the nucleus at the end. The virus thus provides an ideal system for studying the two-way traffic through the nuclear pores.

ACKNOWLEDGMENTS

We thank Carol Featherstone, Larry Gerace, Thomas Kreis, Mark Krystal, and Robert G. Webster for antibodies and Robert Krug for virus stocks. We are most grateful to Helana Hoover-Litty, Philippe Male, and Hans Stukenbrok for excellent technical assistance. We thank Christine Howe and Martina Ittensohn for assistance in preparing ascites and Jonathon Izant for use of his microinjection needle puller. The Yale Statlab provided helpful statistical consultation. We thank Mark Barad and Ila Singh for critical reading of the manuscript and all of the members of the Helenius and Mellman laboratories for advice and criticism.

This work was funded by a U.S. Public Health Service grant from the National Institutes of Health to A.H. (AI18599), and K.M. was supported by the Medical Scientist Training Program.

REFERENCES

1. **Adam, S. A., T. J. Lobl, M. A. Mitchell, and L. Gerace.** 1989. Identification of specific binding proteins for a nuclear location sequence. Nature (London) **337**:276–279.
2. **Batterson, W., D. Furlong, and B. Roizman.** 1983. Molecular genetics of herpes simplex virus. VIII. Further characterization of a temperature-sensitive mutant defective in release of viral DNA and in other stages of the viral reproductive cycle. J. Virol. **45**:397–407.
3. **Beckers, C. J. M., D. S. Keller, and W. E. Balch.** 1987. Semi-intact cells permeable to macromolecules: use in reconstitution of protein transport from the endoplasmic reticulum to the Golgi complex. Cell **50**:523–534.
4. **Bowerman, B., P. O. Brown, J. M. Bishop, and H. E. Varmus.** 1989. A nucleoprotein complex mediates the integration of retroviral DNA. Genes Dev. **3**:469–478.
5. **Choppin, P. W., and R. W. Compans.** 1975. The structure of influenza virus, p. 15–51. *In* E. D. Kilbourne (ed.), The influenza viruses and influenza. Academic Press, Inc., New York.
6. **Compans, R. W., J. Content, and P. H. Duesberg.** 1972. Structure of the ribonucleoprotein of influenza virus. J. Virol. **10**:795–800.
7. **Dales, S., and Y. Chardonnet.** 1973. Early events in the interaction of adenoviruses with HeLa cells. IV. Association with microtubules and the nuclear pore complex during vectorial movement of the inoculum. Virology **56**:465–483.
8. **Davey, J., N. J. Dimmock, and A. Colman.** 1985. Identification of the sequence responsible for the nuclear accumulation of the influenza virus nucleoprotein in Xenopus oocytes. Cell **40**:667–675.
9. **Dingwall, C., and R. A. Laskey.** 1986. Protein import into the cell nucleus. Annu. Rev. Cell Biol. **2**:367–390.
10. **Dworetzky, S. I., and C. M. Feldherr.** 1988. Translocation of RNA-coated gold particles through the nuclear pores of oocytes. J. Cell Biol. **106**:575–584.
11. **Dworetzky, S. I., R. E. Lanford, and C. M. Feldherr.** 1988. The effects of variations in the number and sequence of targeting signals on nuclear uptake. J. Cell Biol. **107**:1279–1287.
12. **Featherstone, C., M. K. Darby, and L. Gerace.** 1988. A monoclonal antibody against the nuclear pore complex inhibits nucleocytoplasmic transport of protein and RNA in vivo. J. Cell Biol. **107**:1289–1297.
13. **Finlay, D. R., D. D. Newmeyer, T. M. Price, and D. J. Forbes.** 1987. Inhibition of in vitro nuclear transport by a lectin that binds to nuclear pores. J. Cell Biol. **104**:189–200.
14. **Froshauer, S., J. Kartenbeck, and A. Helenius.** 1988. Alphavirus RNA replicase is located on the cytoplasmic surface of endosomes and lysosomes. J. Cell Biol. **107**:2075–2086.
15. **Georgatos, S. D., and G. Blobel.** 1987. Lamin B constitutes an intermediate filament attachment site at the nuclear envelope. J. Cell Biol. **105**:117–125.
16. **Heggeness, M. H., P. R. Smith, I. Ulmanen, R. M. Krug, and P. W. Choppin.** 1982. Studies on the helical nucleocapsid of influenza virus. Virology **118**:466–470.
17. **Herz, C., E. Stavnezer, R. M. Krug, and T. J. Gurney.** 1981. Influenza virus, an RNA virus, synthesizes its messenger RNA in the nucleus of infected cells. Cell **26**:391–400.
18. **Hsu, M. T., J. D. Parvin, S. Gupta, M. Krystal, and P. Palese.** 1987. Genomic RNAs of influenza viruses are held in a circular conformation in virions and in infected cells by a terminal panhandle. Proc. Natl. Acad. Sci. USA **84**:8140–8144.
19. **Jennings, P. A., J. T. Finch, G. Winter, and J. S. Robertson.** 1983. Influenza virus ribonucleoprotein guide sequence rear-

rangements in influenza viral RNA? Cell **34**:619–627.
20. **Jones, I. M., P. A. Reay, and K. L. Philpott.** 1986. Nuclear location of all three influenza polymerase proteins and a nuclear signal in polymerase PB2. EMBO J. **5**:2371–2376.
21. **Kalderon, D., B. L. Roberts, W. D. Richardson, and A. E. Smith.** 1984. A short amino acid sequence able to specify nuclear location. Cell **39**:499–509.
22. **Kielian, M., and A. Helenius.** 1986. Entry of alphaviruses, p. 91–119. *In* S. Schlesinger and M. J. Schlesinger (ed.), Togaviridae and Flaviviridae. Plenum Publishing Corp., New York.
23. **Koff, W. C., and V. Knight.** 1979. Inhibition of influenza virus uncoating by rimantadine hydrochloride. J. Virol. **31**:261–263.
24. **Kreis, T.** 1987. Microtubules containing detyrosinated tubulin are less dynamic. EMBO J. **6**:2597–2606.
25. **Laemmli, U. K.** 1970. Cleavage of structural proteins during the assembly of the head of bacteriophage T4. Nature (London) **227**:680–685.
26. **Lamb, R. A., and P. W. Choppin.** 1983. The gene structure and replication of influenza virus. Annu. Rev. Biochem. **52**:467–506.
27. **Lewis, V., S. Green, M. Marsh, P. Vihko, A. Helenius, and I. Mellman.** 1985. Glycoproteins of the lysosomal membrane. J. Cell Biol. **100**:1839–1847.
28. **Lin, B. C., and C. J. Lai.** 1983. The influenza virus nucleoprotein synthesized from cloned DNA in a simian virus 40 vector is detected in the nucleus. J. Virol. **45**:434–438.
29. **Lowry, O. H., N. J. Rosebrough, A. L. Farr, and R. J. Randall.** 1951. Protein measurement with the Folin phenol reagent. J. Biol. Chem. **193**:265–275.
30. **Marsh, M., and A. Helenius.** 1989. Virus entry into animal cells. Adv. Virus Res. **36**:107–151.
31. **Marsh, M., J. Wellsteed, H. Kern, E. Harms, and A. Helenius.** 1982. Monensin inhibits Semliki Forest virus penetration into culture cells. Proc. Natl. Acad. Sci. USA **79**:5297–5301.
31a. **Martin, K., and A. Helenius.** Unpublished data.
32. **Matlin, K. S., H. Reggio, A. Helenius, and K. Simons.** 1982. Infectious entry pathway of influenza virus in a canine kidney cell line. J. Cell Biol. **91**:601–613.
33. **Matteoni, R., and T. Kreis.** 1987. Translocation and clustering of endosomes and lysosomes depends on microtubules. J. Cell Biol. **105**:1253–1256.
34. **Mellman, I., R. Fuchs, and A. Helenius.** 1985. Acidification of endocytic and exocytic pathways. Annu. Rev. Biochem. **55**: 663–700.
35. **Meyer, T., and M. A. Horisberger.** 1984. Combined action of mouse α and β interferons in influenza virus-infected macrophages carrying the resistance gene *Mx*. J. Virol. **49**:709–716.
36. **Murti, K. G., R. G. Webster, and I. M. Jones.** 1988. Localization of RNA polymerases on influenza viral ribonucleoproteins by immunogold labeling. Virology **164**:562–566.
37. **Newmeyer, D. D., and D. J. Forbes.** 1989. Nuclear import can be separated into distinct steps in vitro: nuclear pore binding and translocation. Cell **52**:641–653.
38. **Okhuma, S., and B. Poole.** 1978. Fluorescence probe measurement of the intralysosomal pH in living cells and the perturbation of pH by various agents. Proc. Natl. Acad. Sci. USA **75**:3327–3331.
39. **Peters, R.** 1986. Fluorescence microphotolysis to measure nucleocytoplasmic transport and intracellular mobility. Biochem. Biophys. Acta **864**:305–359.
40. **Rees, P. J., and N. J. Dimmock.** 1981. Electrophoretic separation of influenza virus ribonucleoproteins. J. Gen. Virol. **53**:125–132.
41. **Richardson, W. D., A. D. Mills, S. M. Dilworth, R. A. Laskey, and C. Dingwall.** 1988. Nuclear protein migration involves two steps: rapid binding at the nuclear envelope followed by slower translocation through nuclear pores. Cell **52**:655–664.
42. **Roberts, B. L., W. D. Richardson, and A. E. Smith.** 1987. The effect of protein context on nuclear location signal function. Cell **50**:465–475.
43. **Rodriguez-Boulan, E.** 1983. Polarized assembly of enveloped viruses from cultured epithelial cells. Methods Enzymol. **98**: 487–501.
43a. **Schmid, S.** Unpublished data.
44. **Silver, P., I. Sadler, and M. A. Osborne.** 1989. Yeast proteins that recognize nuclear localization sequences. J. Cell Biol. **109**:983–989.
45. **Simons, K., and H. Virta.** 1987. Perforated MDCK cells support intracellular transport. EMBO J. **6**:2241–2247.
46. **Smith, G. L., J. Z. Levin, P. Palese, and B. Moss.** 1987. Synthesis and cellular location of the ten influenza polypeptides individually expressed by recombinant vaccinia viruses. Virology **160**:336–345.
47. **Snow, C. M., A. Senior, and L. Gerace.** 1987. Monoclonal antibodies identify a group of nuclear pore complex glycoproteins. J. Cell Biol. **104**:1143–1156.
48. **Stegmann, T., R. W. Doms, and A. Helenius.** 1989. Protein-mediated membrane fusion. Annu. Rev. Biophys. Biophys. Chem. **18**:187–211.
49. **Tognon, M., D. Furlong, A. J. Conley, and B. Roizman.** 1981. Molecular genetics of herpes simplex virus. V. Characterization of a mutant defective in ability to form plaques at low temperatures and in a viral function which prevents accumulation of coreless capsids at nuclear pores late in infection. J. Virol. **40**:870–880.
50. **van Wyke, K. L., W. J. J. Bean, and R. G. Webster.** 1981. Monoclonal antibodies to the influenza A virus nucleoprotein affecting RNA transcription. J. Virol. **39**:313–317.
51. **van Wyke, K. L., V. S. Hinshaw, W. J. J. Bean, and R. G. Webster.** 1980. Antigenic variation of influenza A virus nucleoprotein detected with monoclonal antibodies. J. Virol. **35**:24–30.
52. **White, J. M.** 1990. Viral and cellular membrane fusion proteins. Annu. Rev. Physiol. **52**:675–697.
53. **Yoneda, Y., N. Imamoto-Sonobe, Y. Matsuoka, R. Iwamoto, Y. Kiho, and T. Uchida.** 1988. Antibodies to Asp-Asp-Glu-Asp can inhibit transport of nuclear proteins into the nucleus. Science **242**:275–278.
54. **Yoneda, Y., N. Imamoto-Sonobe, M. Yamaizumi, and T. Uchida.** 1987. Reversible inhibition of protein import into the nucleus by wheat germ agglutinin injected into cultured cells. Exp. Cell Res. **173**:586–595.
55. **Yoshimura, A., and S. I. Ohnishi.** 1984. Uncoating of influenza virus in endosomes. J. Virol. **51**:497–504.
56. **Zvonarjev, A. Y., and Y. Z. Ghendon.** 1980. Influence of membrane (M) protein on influenza A virus virion transcriptase activity in vitro and its susceptibility to rimantadine. J. Virol. **33**:583–586.